Morphology optimization via side chain engineering enables all-polymer solar cells with excellent fill factor and stability

Morphology Optimization via Side Chain Engineering Enables All-Polymer Solar Cells with Excellent Fill Factor and Stability

Xi Liu,[†,#] Chaohong Zhang,[‡] Chunhui Duan,[*,†,▽] Mengmeng Li,[▽] Zhicheng Hu,[†] Jing Wang,[§] Feng Liu,[*,§] Ning Li,[‡] Christoph J. Brabec,[‡,^] René A. J. Janssen,[▽] Guillermo C. Bazan,[#] Fei Huang,[*,†] and Yong Cao[†]

[†]Institute of Polymer Optoelectronic Materials and Devices, State Key Laboratory of Luminescent Materials and Devices, South China University of Technology, Guangzhou 510640, P. R. China

[‡]Institute of Materials for Electronics and Energy Technology (i-MEET), Friedrich-Alexander-Universität Erlangen-Nürnberg, Martensstrasse 7, 91058 Erlangen, Germany

[▽]Molecular Materials and Nanosystems, Institute for Complex Molecular Systems, Eindhoven University of Technology, P.O. Box 513, 5600 MB Eindhoven, The Netherlands

[§]Department of Physics and Astronomy, Shanghai Jiao Tong University, Shanghai 200240, P. R. China

[#]Center for Polymers and Organic Solids, University of California, Santa Barbara, California 93106, United States

^Bavarian Center for Applied Energy Research (ZAE Bayern), Immerwahrstrasse 2, 91058 Erlangen, Germany

KEYWORDS: all-polymer solar cells, side chain engineering, morphology, device performance, stability

ABSTRACT: All-polymer solar cells (all-PSCs) composed of conjugated polymers as both donor and acceptor components in bulk heterojunction photoactive layers have attracted increasing attention. However, it is a big challenge to achieve optimal morphology in polymer:polymer blends. In response, we report herein a new strategy to adjust the nanoscale organization for all-PSCs. Specifically, side chain engineering of the well-known naphthalene diimide (NDI) based polymer N2200 is modulated by introducing a fraction of linear oligoethylene oxide (OE) side chains to replace branched alkyl chains on the NDI units and by synthesizing a series of NDI-based polymer acceptors NOE*x*, where *x* is the percentage of OE chain substituted NDI units relative to total NDI units. Compared to the reference polymer NOE0, an OE chain-containing polymer NOE10 offers a much higher power conversion efficiency (PCE) of 8.1% with a

record high fill factor (FF) of 0.75 in all-PSCs. Moreover, the NOE10-based all-PSCs exhibits excellent long-term and thermal stabilities with >97% of the initial PCE being maintained after 300 hours aging at 65 °C. This work demonstrates an effective morphology optimization strategy to achieve highly efficient and stable all-PSCs and shows the excellent potential of NOE10 as an alternative to commercially available acceptor polymers N2200.

■ INTRODUCTION

All-polymer solar cells (all-PSCs) composed of a polymeric electron donor and a polymeric electron acceptor have attracted increasing attention. Compared to the extensively studied polymer:fullerene counterparts, all-PSCs may provide critical advantages, including strong light absorption across a wide spectral region, excellent morphological stability and mechanical durability.[1-3] Moreover, all-PSCs provide unique opportunities to optimize efficiency via tuning and matching optical absorption, energy levels, and the molecular orientation of blend components.[2] Particularly, the open-circuit voltage (V_{oc}) and short-circuit current density (J_{sc}) can be significantly increased. These factors have led to the power conversion efficiencies (PCEs) of all-PSCs to rise from 2% to about 8–10% over the past five years.[4,5] All-PSCs nonetheless still lag behind fullerene-based and the emerging small-molecular non-fullerene PSCs in device performance;[6] very limited all-PSCs offer PCEs over 8%.[5] Principally, the unsatisfied device efficiency is due to the difficulty in controlling the bulk-heterojunction (BHJ) morphology of polymer:polymer blends, resulting in unfavorable charge generation or

transport. Such suboptimal morphology is exemplified by commonly observed low fill factor (FF) values. Indeed, the FF of all-PSCs seldom exceed 0.70, seriously limiting the PCEs of all-PSCs.[5a,5d,5e,5f,5i,7]

A critical effort to realize optimal blend film morphology and high FF for all-PSCs revolves around the development of novel photoactive layer materials. Benefitting from activities in high-performance fullerene-based PSCs, several polymer donors have been developed that offer multiple options of donor materials.[5a,5d,5f,8] State-of-the-art polymer acceptors are also very much in demand for efficient and stable all-PSCs. A few promising polymer acceptors have been reported based on fragments that include naphthalene diimide (NDI),[8b,9] perylene diimide (PDI),[5b,10] bithiophene imide (BTI),[11] double B←N bridged bipyridine (BNBP),[12] and 3,4-difluorothiophene ([2F]T),[13] which offered PCEs over 6%. NDI-based polymers have been most widely investigated due to their high electron affinity, electron mobility, and broad optical absorption. The most well studied NDI-based polymer is poly[[*N*,*N*′-bis(2-octyldodecyl)-naphthalene-1,4,5,8-bis(dicarboximide)-2,6-diyl]-*alt*-5,5′-(2,2′-bithiophene)] with the commercial name N2200,[14] which afforded the PCE record of all-PSCs so far.[5f] Based on these considerations, the further development and design of novel polymers based on NDI will not only likely afford promising acceptor materials, but also have an important impact on achieving well controlled BHJ morphology via rational polymer design.

Herein, we report a new strategy to adjust the nanoscale morphology of the blend film for all-PSCs. A series of new NDI-based polymer acceptors were developed by

introducing a fraction of linear oligoethylene oxide (OE) side chain to replace the branched alkyl chain on the NDI units. It has been reported that introducing OE side chains onto the photoactive materials can adjust polymer crystallization, charge carrier mobility, and donor:acceptor miscibility in blends.[15] The polymers are denoted as NOE*x*, where *x* stands for the molar percentage of OE chain substituted NDI units relative to the total NDI units. As shown in Figure 1, the molar percentage of the OE chain substituted NDI units is set to be 10%, 20%, and 30%, leading to polymers NOE10, NOE20, and NOE30, respectively. Notably, the commercial name of the OE chain-free reference polymer NOE0 is N2200. We found that the introduction of OE side chains has little influence on the optical and electrochemical properties, but can substantially change the surface energies and crystallinity in the bulk. Compared to NOE0, NOE10 offers a much higher PCE of 8.1% with a higher J_{sc} of 12.9 mA cm^{-2} and a record high FF of 0.75 by using PBDT-TAZ (Figure 1) as the donor component of the blend.[16] This FF is among the highest values reported so far for all-PSCs, approaching the highest FF of 0.80 in fullerene-based PSCs,[5i,17] and suggesting the great opportunity of efficiency optimization in all-PSCs. Further investigation revealed that favorable BHJ morphology with proper phase separation and vertical gradient distribution were enabled by NOE10, which is the main reason for the impressive device performance. Moreover, NOE10-based all-PSCs demonstrated excellent long-term stabilities and thermal stabilities, exhibiting superiority relative to other high-efficiency solution processed organic photovoltaics. Overall, the results obtained in this work not only provide an effective strategy for morphology and efficiency optimization of all-PSCs, but also

suggest the outstanding potential of all-PSCs for future technological applications.

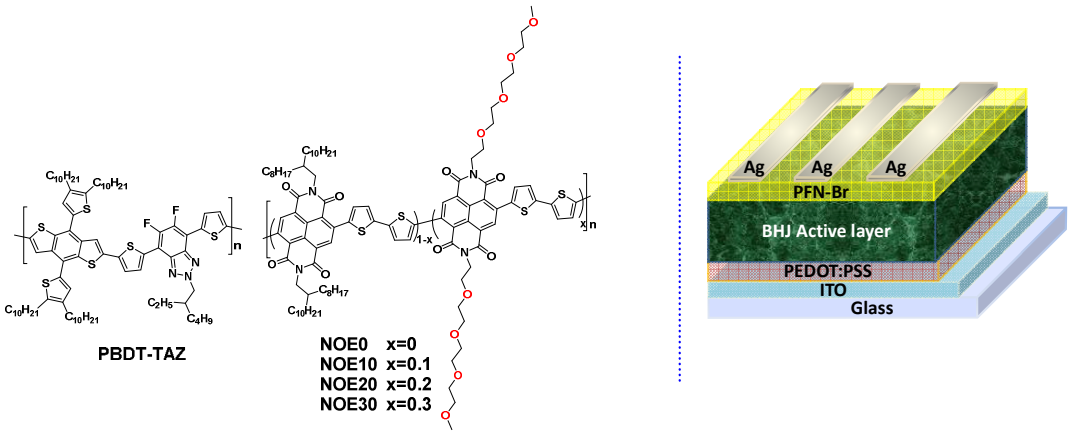

Figure 1. The chemical structures of the donor and acceptor polymers, and the device architecture of all-PSCs employed in this study.

■ RESULTS AND DISCUSSION

Design, Synthesis, and Characterization of NOE*x*

Our design for new polymer acceptors is based on N2200, which is a widely used *n*-type polymer due to its high electron affinity and electron mobility.[14] Different molar percentages of OE chain modified NDI unit were used as the third monomer in the copolymerization reaction, affording four polymers NOE0, NOE10, NOE20, and NOE30 (Figure 1). These four polymers contain the same conjugated main chain to ensure efficient electron transport, while the OE side chains were anticipated to fine tune miscibility and morphology of the polymer:polymer blend films. The synthetic route (Figure S1, Supporting Information) and detailed procedures for the preparation of the four polymers are described in the Supporting Information. The polymers were synthesized by Stille cross-coupling polymerization from three monomers, 4,9-dibromo-2,7-bis(2-octyldodecyl)benzo[lmn][3,8]phenanthroline-1,3,6,8(2H,7H)-tet

raone (NDIBr-C8C12), 4,9-dibromo-2,7-di(2,5,8,11-tetraoxatridecan-13-yl)benzo[lmn][3,8]phenanthroline-1,3,6,8(2H,7H)-tetraone (NDIBr-OE), and 5,5′-bis(trimethylstannyl)-2,2′-bithiophene (2ThSn) with corresponding feed ratios. The resulting products can be readily dissolved at room temperature in common organic solvents, such as chloroform (CF), chlorobenzene (CB), and 1,2-dichlorobenzene (DCB). Gel permeation chromatography (GPC) measurements in 1,2,4-trichlorobenzene at 150 °C showed that the polymers have similar number average molecular weights (M_n) of ~80 kDa and polydispersity index (PDI) of ~2.0; see Table 1 and Figure S2 in the Supporting Information. Introducing OE side chains has little influence on solubilities and molecular weights of the resulting polymers, thereby ensuring a fair comparison for their performance in all-PSCs.

The optical absorption properties of the acceptor polymers (NOE0, NOE10, NOE20, and NOE30), the donor polymer PBDT-TAZ, and the corresponding blend films were recorded via UV–vis–NIR absorption spectroscopy. The resulting spectra are shown in Figure 2a and Figure S3 (Supporting Information), and relevant data are listed in Table 1. Introducing OE side chains leads to negligible changes relative to the fully alkylated reference polymer NOE0. All polymers show absorption peaks at 707 and 393 nm, with onsets at ~850 nm, leading to optical band gaps (E_g^{opt}) estimated to be 1.46 eV. The absorption coefficients of all acceptor polymers are similar (Figure S3c, Supporting Information), suggesting that the OE side chains have little influence on the light absorption of the materials. Considering the narrow bandgap of the acceptor polymers, a wide bandgap polymer (PBDT-TAZ) was selected as the electron donor for all-PSCs,[16]

to maximize the light harvesting ability of the blends (Figure 2a and Figure S3b in the Supporting Information).

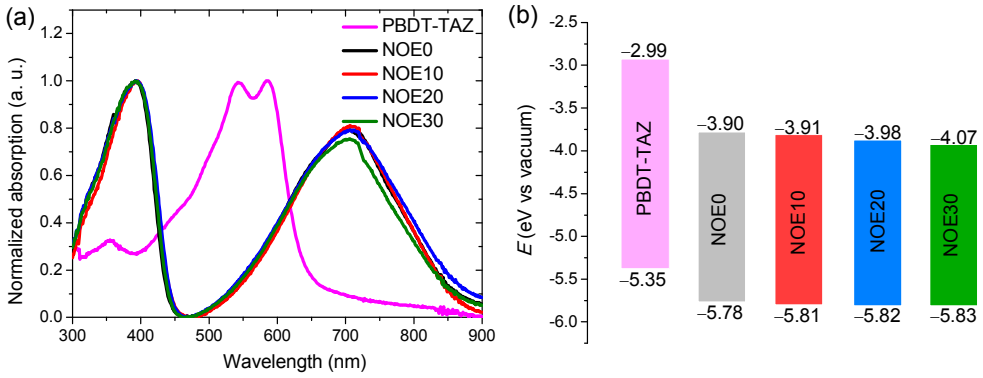

Figure 2. (a) The optical absorption spectra of PBDT-TAZ, NOE0, NOE10, NOE20, and NOE30 in films; (b) energy levels of PBDT-TAZ, NOE0, NOE10, NOE20, and NOE30.

Table 1. Molecular weights, optical properties, and energy levels of the donor and acceptors polymers.

Polymers	M_n [kDa]	PDI	λ_{max} [a)] [nm]	λ_{onset} [a)] [nm]	E_g^{opt} [b)] [eV]	E_{ox} [V]	E_{re} [V]	E_{HOMO} [c)] [eV]	E_{LUMO} [d)] [eV]
PBDT-TAZ	29	2.5	586, 544	641	1.93	0.83	–1.53	–5.35	–2.99
NOE0	84	1.8	707, 393	847	1.46	1.26	–0.62	–5.78	–3.90
NOE10	83	2.0	707, 393	850	1.46	1.29	–0.61	–5.81	–3.91
NOE20	97	2.4	707, 393	852	1.46	1.30	–0.54	–5.82	–3.98
NOE30	78	2.3	707, 393	852	1.46	1.31	–0.45	–5.83	–4.07

[a)]In films; [b)]$E_g^{opt} = 1240/\lambda_{onset}$; [c)]$E_{HOMO} = -[4.80 - E_{Ferrocene} + E_{ox}]$; [d)]$E_{LUMO} = -[4.80 - E_{Ferrocene} + E_{re}]$, $E_{Ferrocene} = 0.28$ V.

Electrochemical properties were investigated by cyclic voltammetry (CV) (Figure S3d, Supporting Information). Relevant data from these studies are listed in Table 1, and the resulting estimated energy diagram of the polymers is depicted in Figure 2b. The highest occupied molecular orbital (HOMO) of the OE chains-containing polymers (around –5.80 eV) are close to that of NOE0. The lowest unoccupied molecular orbital (LUMO) of the acceptor polymers are slightly lowered by introducing OE side chains as

compared to the reference polymer NOE0, which might be due to the weak electron-donating effect of the OE side chains to the polymer backbone.[15a] Each PBDT-TAZ:NOE*x* combination has sufficient energy offsets (>0.3 eV) for efficient exciton dissociation at donor:acceptor interfaces.[18]

Contact angle measurements were performed to examine the surface energies of the films.[19] The relevant images are shown in Figure S4 (Supporting Information) and the parameters are summarized in Table S1.[20] By adding more OE chains onto the acceptor polymer, both the water contact angle and oil contact angle become smaller due to the amphiphilicity of OE chains. As a result, introducing more OE chains leads to enhanced contributions from dispersion force but reduced contributions from polar force for the polymer surface energies. Overall, the surface energies of the three OE chain-containing polymers are very similar among each other, but are greatly higher than the reference polymer NOE0. Flory–Huggins interaction parameter $\chi_{donor,acceptor}$ representing the interaction between the polymer donor and polymer acceptor is a critical evaluation index for polymer:polymer miscibility.[21] A low $\chi_{donor,acceptor}$ value means good polymer:polymer miscibility, while a high $\chi_{donor,acceptor}$ value tends to trigger phase separation in blend films. Estimates for $\chi_{donor,acceptor}$ can in principle be derived using the empirical equation of $\chi_{donor,acceptor} = K(\sqrt{\gamma_{donor}} - \sqrt{\gamma_{acceptor}})^2$, where K is a constant, γ_{donor} and $\gamma_{acceptor}$ are the surface energies of the neat films of donor polymer and acceptor polymer, respectively.[21d] As shown in Table S1, the three OE chain-containing polymers lead to similar $(\sqrt{\gamma_{donor}} - \sqrt{\gamma_{acceptor}})^2$ values in blends, which are caused by their similar surface energies. However, the $(\sqrt{\gamma_{donor}}$ –

$\sqrt{\gamma_{\text{acceptor}}})^2$ values are reduced significantly from 0.051 for the reference polymer acceptor NOE0 to ≈0.020 for the OE chain-containing polymers, suggesting that the OE chain-containing polymers are more miscible with PBDT-TAZ than NOE0. One can therefore expect the phase separation in polymer:polymer blends to be modified by introducing OE side chains on the acceptor polymer. More detailed discussion on the morphology of all-polymer blends will be given in the following parts.

Photovoltaic Properties

Bulk heterojunction all-PSCs based on the donor polymer PBDT-TAZ and the NOE*x* polymer acceptors were fabricated with a device structure of ITO/PEDOT:PSS/PBDT-TAZ:NOE*x*/PFN-Br/Ag. The device performance for PBDT-TAZ:NOE0 and PBDT-TAZ:NOE10 was firstly optimized in donor:acceptor weight ratio while keep other conditions constant, which suggested an optimal ratio of 2:1 for the both blends. The PBDT-TAZ:NOE10 blend was further optimized in terms of amount, and type of solvent additive, and thermal annealing at different temperatures to maximize the PCE. The blend films that spin-coated from a solvent mixture of chloroform with 2% diphenyl ether in volume and further annealed at 160 °C for 5 min before depositing metal electrode gave the best device performance. These optimal conditions established on PBDT-TAZ:NOE10 were then extended to other donor:acceptor blends, and the results from different fabricating conditions are shown in Table S2 in the Supporting Information. Solar cells of PBDT-TAZ:NOE0 and PBDT-TAZ:NOE10 with a inverted structure of ITO/ZnO/active layer/MoO_3/Ag were also tested, which all produced poorer results (Table S3). Current density–voltage (*J*–*V*)

curves and external quantum efficiency (EQE) spectra of the best devices for each polymer acceptor are shown in Figure 3a and 3b. Champion device results, average values, and standard deviations of device statistics from twelve independent devices for each acceptor polymer are listed in Table 2.

The PBDT-TAZ:NOE0 solar cell shows a PCE of 6.8% with a V_{oc} of 0.86 V, J_{sc} of 11.4 mA cm^{-2}, and FF of 0.69, consistent with the reported results from similar active layer.[8b] Compared to the PBDT-TAZ:NOE0 solar cell, the performance of PBDT-TAZ:NOE10 solar cell is significantly enhanced and achieves a PCE of 8.1% with a higher J_{sc} of 12.9 mA cm^{-2}, and an FF of 0.75. To the best of our knowledge, this FF is among the highest values reported for all-PSCs, approaching the highest FF of 0.80 attained with fullerene-based PSCs.[5i,17] The PBDT-TAZ:NOE20 solar cell also offers a PCE of 7.3%, associated with a J_{sc} of 11.9 mA cm^{-2} and an impressive FF of 0.73. The PBDT-TAZ:NOE30 solar cell shows a modest PCE of 6.1% as a result of lower V_{oc} and J_{sc} values. Notably, the V_{oc} of the all-PSCs decreased slightly upon introducing OE side chains onto the acceptor polymers, which agrees with expectations as a result of differences in LUMO levels. Considering the similar absorption coefficients of the four blend films (Figure S3c, Supporting Information), the significantly higher J_{sc} and FF of the NOE10-based all-PSCs are most reasonably attributed to optimization of the BHJ morphology. To further demonstrate the potential of NOE10 for all-PSCs, the widely used donor polymer PCE10 was also selected to fabricate all-PSCs. As shown in Figure S5 and Table S4 (Supporting Information), the PCE10:NOE10 solar cells show a PCE of 6.4%, which is higher than the PCE10:NOE0 based device (with a PCE of 5.1%). Hence,

NOE10 shows a broad applicability to match different polymer donors. Altogether, these results demonstrate that NOE10 is a promising alternative to the commercial polymer N2200 for the fabrication of all-PSCs.

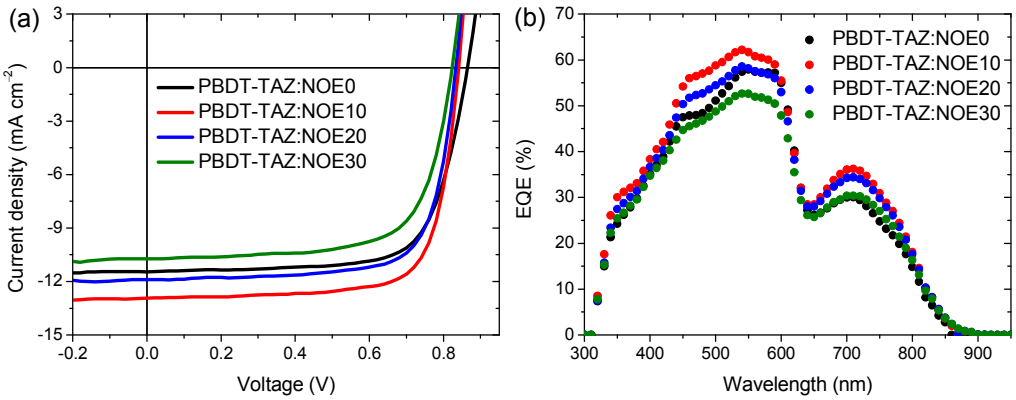

Figure 3. (a) Current density–voltage characteristics of the all-PSCs under AM1.5G illumination at 100 mW cm^{-2}; (b) EQE spectra of the corresponding all-PSCs devices.

Table 2. Photovoltaic properties of the all-PSCs under AM1.5G illumination at 100 mW cm^{-2}.

Active layer[a)]	V_{oc}[b)] [V]	J_{sc}[b)] [mA cm^{-2}]	$J_{sc,\ EQE}$[c)] [mA cm^{-2}]	FF[b)]	PCE[b)] [%]
PBDT-TAZ:NOE0	0.86 (0.86 ± 0.01)	11.4 (11.2 ± 0.2)	10.8	0.69 (0.69 ± 0.02)	6.8 (6.8 ± 0.1)
PBDT-TAZ:NOE10	0.84 (0.84 ± 0.01)	12.9 (12.4 ± 0.5)	12.2	0.75 (0.75 ± 0.01)	8.1 (7.9 ± 0.2)
PBDT-TAZ:NOE20	0.83 (0.83 ± 0.01)	11.9 (11.8 ± 0.1)	11.5	0.73 (0.72 ± 0.01)	7.3 (7.1 ± 0.2)
PBDT-TAZ:NOE30	0.82 (0.82 ± 0.01)	10.7 (10.4 ± 0.3)	10.4	0.69 (0.70 ± 0.01)	6.1 (6.0 ± 0.1)

[a)]The active layers were optimized with a donor:acceptor weight ratio of 2:1 and spin-coated from a solvent mixture of chloroform with 2% diphenyl ether in volume and further annealed at 160 °C for 5 min before electrode deposition; [b)]The average values and standard deviation of device statistics from 12 devices are listed in the parentheses; [c)]photocurrents obtained by integrating the EQE curves.

The EQE spectra of the all-PSCs are shown in Figure 3b. The all-PSCs show broad

photo-response over the spectral region from 300 to 850 nm, which is consistent with the absorption of the blend films. The EQE curves also suggest photocurrent contributions from both donor and acceptors polymers. EQEs peaked at ≈550 nm mainly originate from electron transfer from PBDT-TAZ to the polymer acceptors, and the EQEs peaked at ≈710 nm are attributed to hole transfer from the polymer acceptors to PBDT-TAZ. The photocurrents obtained by integrating the EQE curves are slightly lower than the J_{sc} measured from the *J–V* curves with a mismatch within 5%. Similar to N2200, the low absorption coefficient of NOE*x* in low energy region limit the EQEs and the J_{sc} in solar cells. Further research toward higher PCEs of all-PSCs should thus focus on improving the absorption coefficient in near infrared region, such as adding a narrow bandgap polymer with intense light absorption to form ternary solar cells.

Charge Generation, Transport, and Recombination

Photoluminescence (PL) quenching experiments were conducted to investigate photoinduced charge transfer processes at the donor/acceptor interfaces. Pure films of PBDT-TAZ, NOE0, NOE10, NOE20, NOE30, and the four corresponding blend films were excited at 530 nm to study electron transfer from excited PBDT-TAZ to acceptor polymers and at 710 nm to study hole transfer from excited acceptor polymers to PBDT-TAZ. As shown in Figure S6a (Supporting Information), PBDT-TAZ:NOE10 shows a PL quenching efficiency (96%) that is higher than for the other three blends (76% for PBDT-TAZ:NOE0, 90% for PBDT-TAZ:NOE20, and 90% for PBDT-TAZ:NOE30), suggesting the most efficient electron transfer from the excited donor to NOE10. When excited at 710 nm, the PBDT-TAZ:NOE10 film also shows a higher PL quenching

efficiency (89%) (83% for PBDT-TAZ:NOE0, 81% for PBDT-TAZ:NOE20, and 81% for PBDT-TAZ:NOE30; Figure S6b in the Supporting Information), suggesting the most efficient hole transfer from the excited acceptor to NOE10. The most efficient electron and hole transfer efficiencies in the PBDT-TAZ:NOE10 blend film agree well with the highest EQE and J_{sc} in all-PSCs.

We then studied the exciton dissociation probability $P(E,T)$ of the solar cells.[22] Figure 4a shows the photocurrent density (J_{ph}, $J_{ph} = J_L - J_D$, where J_L and J_D are the light and dark current density, respectively) *versus* effective voltage (V_{eff}, $V_{eff} = V_o - V_a$, where V_o is the voltage when J_{ph} is equal to 0, and V_a is the applied bias voltage) of the all-PSCs. The $P(E,T)$ is defined by normalizing J_{ph} with the saturation photocurrent density (J_{sat}). Under short-circuit conditions, the all-PSCs show $P(E,T)$ values over 93%, suggesting efficient exciton dissociation for all devices. The highest $P(E,T)$ value of 96% was produced by NOE10-based device, consistent with the highest J_{sc} and EQE of the PBDT-TAZ:NOE10 devices. It is worth pointing out that the difference in *P(E,T)* for the various devices is small, so the differences in J_{sc} and EQE are probably rather determined by charge recombination than by generation.

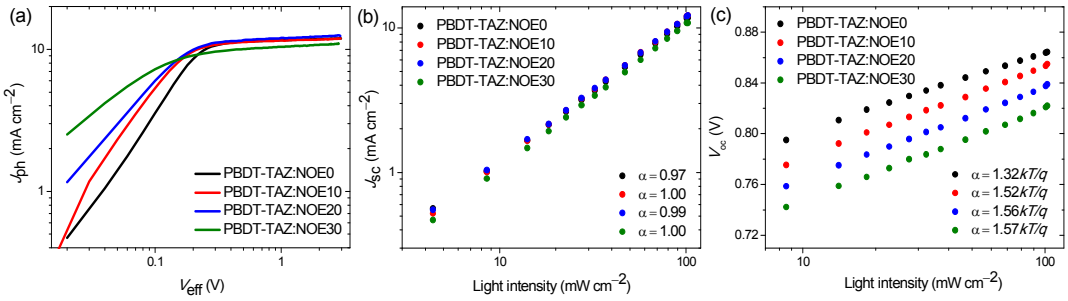

Figure 4. (a) Photocurrent density (J_{ph}) *versus* effective voltage (V_{eff}) curves of the all-PSCs; (b) light intensity dependence of J_{sc} of the all-PSCs; (c) light intensity dependence of V_{oc} of the all-PSCs.

The device performance, especially J_{sc} and FF, is also greatly affected by charge transport and recombination. The charge carrier mobility in pure acceptors and their blend films were thus measured from single carrier devices by fitting the *J*–*V* data to a space-charge-limited current model. The results are summarized in Table S5 (Supporting Information). In pure polymer films, the four NOE*x* polymers exhibit similar electron mobilities (μ_e) of ≈4.0 × 10^{-5} $cm^2 V^{-1} s^{-1}$. After blended with PBDT-TAZ, the NOE10-, NOE20-, and NOE30-based blend films exhibit μ_e of 1.6, 1.5, and 1.2 × 10^{-4} $cm^2 V^{-1} s^{-1}$, respectively, which are considerably higher than the NOE0-based film (5.7 × 10^{-5} $cm^2 V^{-1} s^{-1}$). Additionally, the four blend films show very similar hole mobilities (μ_h) in a range from 2.1 × 10^{-4} to 1.5 × 10^{-4} $cm^2 V^{-1} s^{-1}$. Correspondingly, the μ_e/μ_h ratios for NOE0, NOE10, NOE20, and NOE30 blend films are 0.3, 1.0, 0.9, and 0.8, respectively. The optimally balanced electron/hole transport in the PBDT-TAZ:NOE10 blend contributes to the highest FF and J_{sc} in solar cells

Charge recombination mechanisms of the all-PSCs were examined through measurements of the light intensity dependence of the J_{sc} and V_{oc}. The correlation of the J_{sc} and the light intensity (P_{light}) obeys the power–law $J_{sc} \propto P_{light}^{\alpha}$, where α is an exponential factor that should be equal to 1 if the bimolecular recombination of the device is negligible.[23] As shown in Figure 4b, α values from the fitted line for the all-PSCs based on NOE0, NOE10, NOE20, and NOE30 are 0.97, 1.00, 0.99, and 1.00, respectively, indicating negligible bimolecular recombination in these devices. The slope of V_{oc} *versus* ln(P_{light}) curve reflects the property of charge recombination at open

circuit condition. The slope will be 1.0kT/q when bimolecular recombination is dominant, where k is the Boltzmann constant and T is the temperature.[23] As shown in Figure 4c, the all-PSCs based on NOE0, NOE10, NOE20, and NOE30 exhibit a slope of 1.32kT/q, 1.52kT/q, 1.56kT/q, and 1.57kT/q, respectively. These observations suggest that the OE chain-containing acceptor polymers can reduce bimolecular recombination in all-PSCs.

To evaluate the efficiency of collected carriers per incident absorbed photon upon introducing OE chains onto polymer acceptor, the internal quantum efficiencies (IQEs) of the PBDT-TAZ:NOE0 and PBDT-TAZ:NOE10 solar cells were calculated from their EQEs and the total fraction of absorbed photons, which was determined from the wavelength dependent refractive index and extinction coefficients followed by optical modelling of the entire device stack. As shown in Figure 5, the PBDT-TAZ:NOE10 solar cell shows higher IQEs than PBDT-TAZ:NOE0 cell in the main absorption range of 400–700 nm, suggesting that the absorbed photons are more efficiently converted into free charge carriers in NOE10-based device. For both blends, the contributions of the PBDT-TAZ and NOEx to the IQE are similar, evidencing both components provide equal contributions to photocurrent after absorbing light.

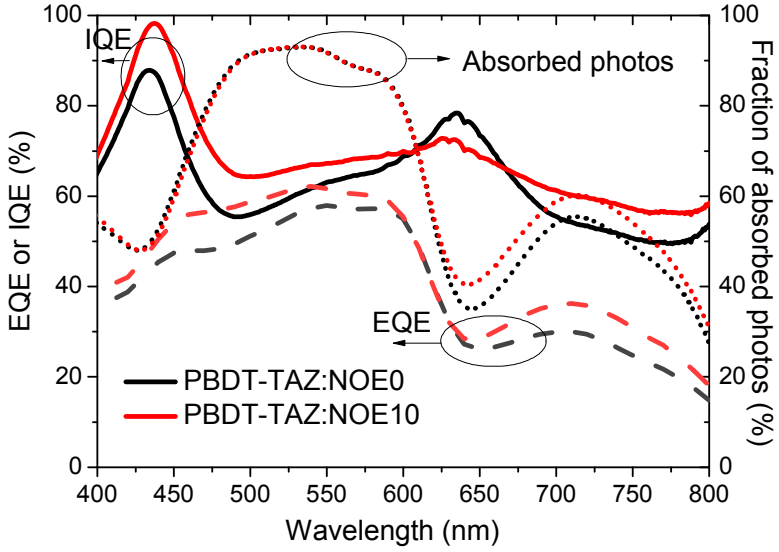

Figure 5. Internal quantum efficiency (IQE) of PBDT-TAZ:NOE0 and PBDT-TAZ:NOE10 based devices (solid lines), EQE curves of the two devices (dash lines), and absorption of the two blend films (short dot lines). The peaks in the IQEs at ~640 nm are possibly due to an underestimation of the fraction absorbed photons.

Morphology

The structural order of pure and blended thin films were investigated by grazing incidence wide-angle x-ray diffraction (GIWAXS) method. The 2D diffraction images and line-cut profiles are shown in Figure S8 (Supporting Information). These studies show that both PBDT-TAZ and the NOE polymer series take a preferred face-on orientation relative to the substrate. PBDT-TAZ showed a (100) diffraction peak in the in-plane direction at ~0.25 Å. The crystal coherence length (CCL) obtained by use of the Scherer equation yielded a value of 12.1 nm. Notably, for the NOE polymer series the relative crystallinity decreases as the content of hydrophilic OE side chain increases. NOE0 shows a quite sharp (100) diffraction at ~0.25 Å, with a CCL of 41.8 nm.

Introducing hydrophilic side chains leads to a reduction of (100) peak intensity and full-width-at-half-maximum (FWHM). NOE10, NOE20, and NOE30 yield CCLs of 36.9, 27.3, and 14.6 nm, respectively. The sharp peak at 0.45 Å in the in-plane direction was assigned to the (001) plane of NOE polymer series. Thus quite rigid backbone and well-ordered side chains can be resolved. It should also be noted that adjacent to this peak comes the (200) diffraction from NOE polymers, which decreases in intensity as the hydrophilic side chain content increases. Pi-pi stacking features can be well-resolved in the out of plane direction. PBDT-TAZ shows a diffraction peak at 1.73 Å, while the NOE polymer series shows diffraction peaks at 1.62 Å. BHJ thin films (Figure 6) show diffraction features that are a combination of features characteristic of PBDT-TAZ and the NOE polymer series. The similar position of (100) diffraction from donor and acceptor polymers made it difficult to evaluate the crystal coherence length of each species. Yet the overall FWHM gradually increased from PBDT-TAZ:NOE0 to PBDT-TAZ:NOE30 blends (size change from 32 to 21 nm). The well-developed (001) peak from NOE polymers indicated that they form good ordered structures in blends. The correlation length of (001) peak was estimated to be 30–40 nm for PBDT-TAZ:NOE blends, which reduces slightly with more hydrophilic OE side chains. Thus good chain alignment in solid-state packing is expected. Weak (300) diffractions were seen from NOE polymers, and thus the good crystallinity and crystal quality should form the framework of phase-separated structure in BHJ blends. The pi-pi stacking of BHJ blended film is located at 1.66–1.68 Å, which summarized packing features from both donor and acceptor polymers. It should be noted that PBDT-TAZ:NOE10 blends show

the smallest packing at 1.66 Å, indicating the highest contribution from NOE10 polymers, and thus best structural order for acceptor polymers in BHJ blends.

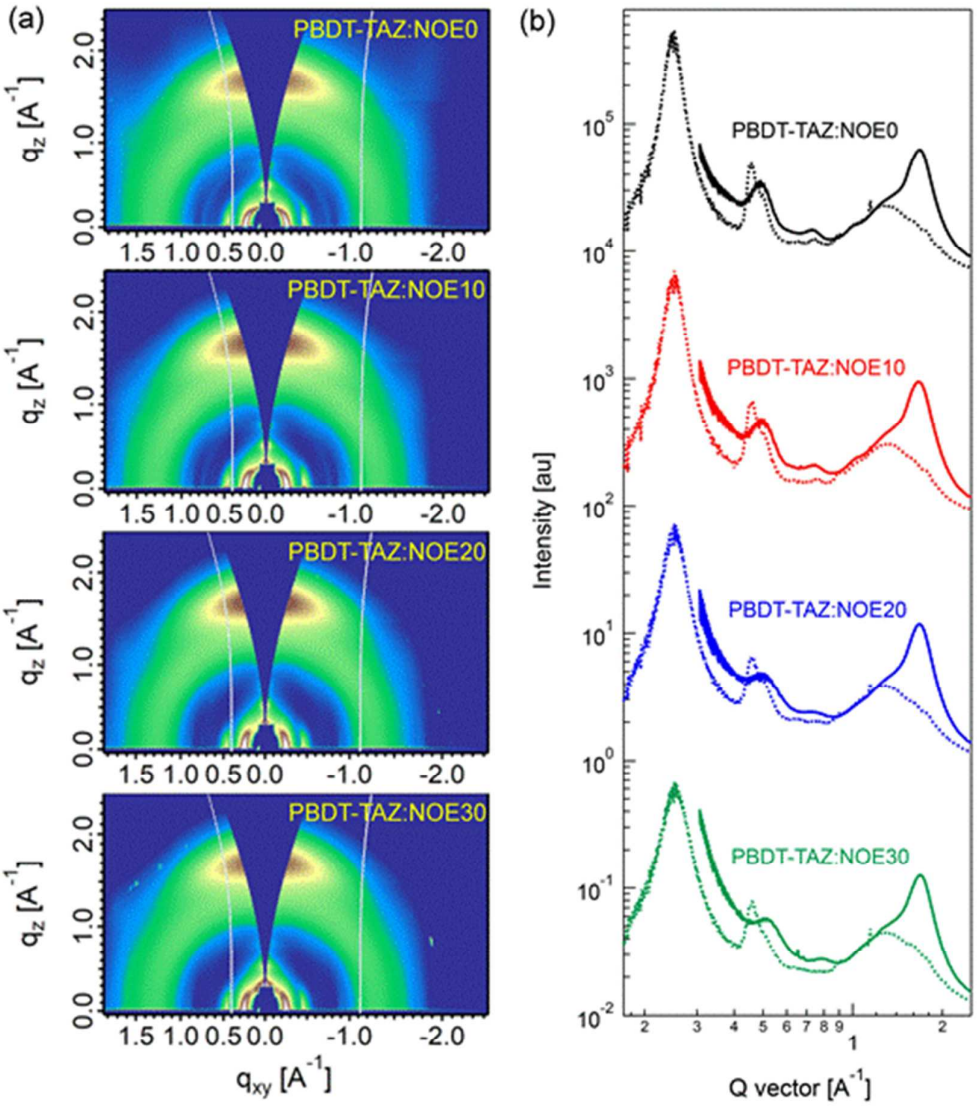

Figure 6. GIWAXS of PBDT-TAZ:NOE*x* BHJ films. Diffraction patterns (a), and line-cut profiles (b) (solid line: out-of-plane line-cut profiles; dotted line: in-plane line-cut profiles).

The morphology of the active layers was studied by transmission electron microscopy (TEM), see Figure 7. Films based on NOE0 and NOE10 blends show

whiskers with diameters of tens of nanometers and lengths of hundreds of nanometers, which are roughly aligned radially, as expected from centrifuge force of spin coating. NOE20 based blend films showed blurred whiskers, and these features became not obvious for NOE30 based blends. These whiskers showed size scales similar to NOE polymers by GIWAXS characterizations. These ordered structures are favorable to efficient charge transport in blend films, and thus contribute to the excellent FF and higher J_{sc} in all-PSCs device. Moreover, such blend morphology is also in favor of long-term stability of the devices, which will be discussed later. TEM images also showed aggregated species with different color depth with roughly 100 nm phase-separated length scales. These features were observed in resonant soft x-ray scattering (RSoXS) experiment (Figure S9, Supporting Information) with diffuse humps. NOE10 and NOE20 based blends showed the least scattering intensity, which indicates better film uniformity. Such a feature added to whiskers morphology can be used to explain the improved device performance with the novel polymer acceptors.

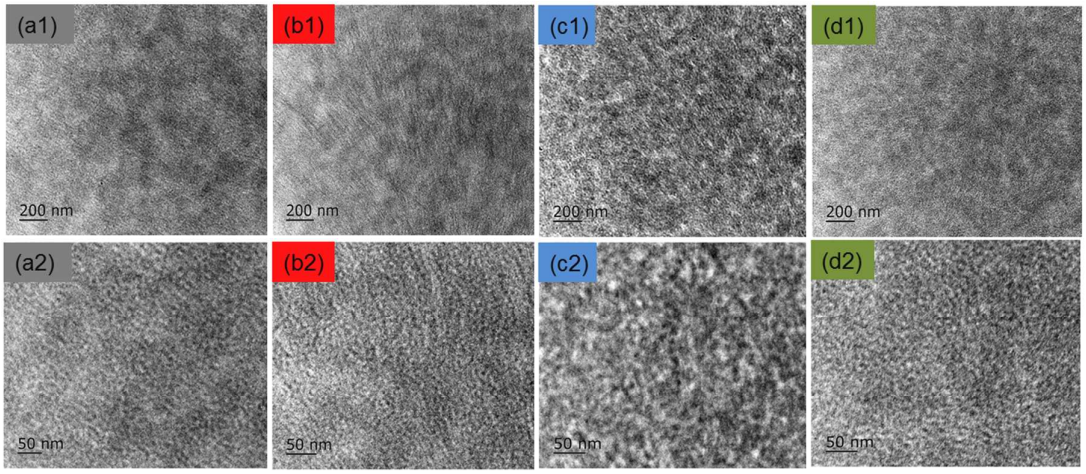

Figure 7. TEM images of the PBDT-TAZ:NOE*x* blend films based on NOE0 (a1,a2), NOE10 (b1,b2), NOE20 (c1,c2), and NOE30 (d1,d2), respectively. The scale bar is 200 nm for a1, b1, c1, and d1, and 50 nm for a2, b2, c2, and d2.

The importance of the nano whisker morphology in PBDT-TAZ:NOE10 blends were further revealed by photoinduced force microscopy (PiFM).[24] By imaging at the characteristic Fourier transform infrared (FT-IR) wavenumber corresponding to absorption peaks of donor and acceptor materials, PiFM showed better resolution power to spatially map nanoscale patterns of specific chemical components in blend films.[5c,25] As shown in Figure S10 (Supporting Information), we selected the absorption peak at 1758 cm^{-1} in FTIR for PBDT-TAZ imaging and the peak at 1668 cm^{-1} for NOE0 and NOE10 imaging in PiFM measurements. As shown in Figure 8a1 and 8b1, when selectively imaged at 1758 cm^{-1} by PiFM, PBDT-TAZ phase was highlighted, which homogenously distributes over the entire films, forming a good hole transporting media. Figure 8a2 and 8b2 present the selective imaging of the blend films at 1668 cm^{-1}, where NOE polymer acceptors were highlighted. Figure 8a3 and 8b3 display the combinations of the PiFM images at 1758 and 1668 cm^{-1} for PBDT-TAZ:NOE0 and PBDT-TAZ:NOE10, respectively. PiFM images with a large length scale demonstrated in Figure 8a4 and 8b4 revealed nano whiskers with diameters of tens of nanometers and length of hundreds of nanometers. Moreover, in NOE10-based blends these nano whiskers were better separated with less agglomerated bundles. Thus there are more internal interfaces for PBDT-TAZ:NOE10 blends, giving rise to improved J_{sc}. It is thus clear that NOE10 can lead to the formation of not only more proper phase separation in all-polymer blends but also more crystalline polymer fibers with more clear grain boundaries, which ultimately contribute to enhanced charge transport and solar cell performance.

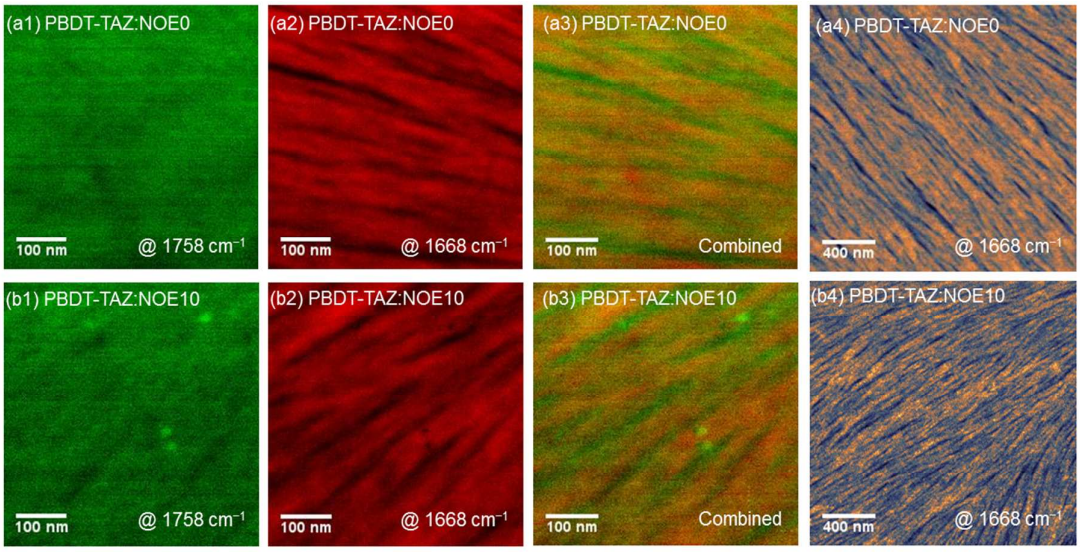

Figure 8. PiFM images of the two blend films. (a1) PBDT-TAZ:NOE0 and (b1) PBDT-TAZ:NOE10 imaged at 1758 cm^{-1}; (a2) PBDT-TAZ:NOE0 and (b2) PBDT-TAZ:NOE10 imaged at 1668 cm^{-1}; (a3) PBDT-TAZ:NOE0 and (b3) PBDT-TAZ:NOE10 by combining the images mapped at 1758 and 1668 cm^{-1}; (a4) PBDT-TAZ:NOE0 and (b4) PBDT-TAZ:NOE10 imaged at 1668 cm^{-1} with larger length scale. The scale bars are shown in each picture.

Secondary ion mass spectrometry (SIMS) is a sensitive surface analytical technique, which can be used to determine the elemental composition of the samples as function of depth. As shown in Figure S11 (Supporting Information), the counts of ^{13}C and ^{16}O in the PBDT-TAZ:NOE0 and PBDT-TAZ:NOE10 blend films were recorded over sputtering time. In the two blend films, we can probe relative vertical phase distribution using the $^{16}O/^{13}C$ count ratios as oxygen element is characteristic for the acceptor polymers. Figure 8a shows the $^{16}O/^{13}C$ count ratios for PBDT-TAZ:NOE0 and PBDT-TAZ:NOE10, which were calculated from Figure S11a and S11b (Supporting Information), respectively. In order to make an accurate comparison, a curve of ($^{16}O/^{13}C$) × 1.2 count ratio was used for PBDT-TAZ:NOE0 because, statistically, the oxygen population of NOE10 is 1.2 times that of NOE0. Within the first 40 nm depth range of the blend films, the $^{16}O/^{13}C$ ratios

of PBDT-TAZ:NOE10 are higher than the ($^{16}O/^{13}C$) × 1.2 ratios of PBDT-TAZ:NOE0, indicating that NOE10 is more prone to be enriched at the active layer surface compared to NOE0. Conversely, for the last 40 nm depth range of the blend films, the $^{16}O/^{13}C$ ratios of PBDT-TAZ:NOE10 are lower than the ($^{16}O/^{13}C$) × 1.2 ratios of PBDT-TAZ:NOE0, suggesting NOE10 is less enriched at the bottom of the active layer than NOE0. In this case, the PBDT-TAZ:NOE10 blend shows more proper vertical phase distribution with the device structure of ITO/PEDOT:PSS/active layer/PFN-Br/Ag, which ultimately facilitates charge extraction and reduces charge recombination; features that combine to produce a higher FF and J_{sc}. Combined with TEM images, PiFM results, and SIMS analysis, we can establish three-dimensional microstructure schematics of the PBDT-TAZ:NOE0 and PBDT-TAZ:NOE10 blends (Figure 9b and 9c), which describe the polymer ordering, phase separation and vertical phase gradation of the two blend films.

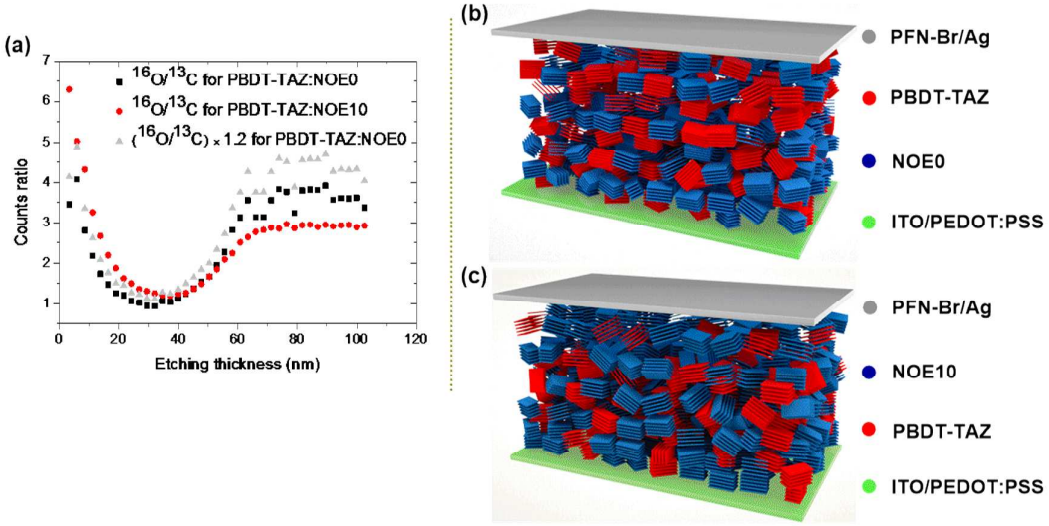

Figure 9. (a) $^{19}F/^{16}O$ counts ratios in the two blend films over thickness; (b) schematic illustration of PBDT-TAZ:NOE0 blend film; (c) schematic illustration of PBDT-TAZ:NOE10 blend film.

Device Stability

It has been previously established that a BHJ morphology with high miscibility of donor phase and acceptor is beneficial to achieve high device stability.[26] We thus expect that PBDT-TAZ:NOE10 blend will exhibit improved device stability in all-PSCs. Accordingly, device stabilities of the PSCs made from the same donor PBDT-TAZ but different acceptors of NOE0, NOE10, PCBM, and ITIC were tested and are compared in Figure 10a and S12 (Supporting Information). NOE0 (N2200), PCBM, and ITIC have been widely used as electron acceptors for organic photovoltaics. Devices were stored in nitrogen-filled glovebox at room temperature under dark conditions. The performances of these devices upon different storage time are shown in Figure S12 (Supporting Information). After 400 hours storage under dark conditions, the PBDT-TAZ:NOE10 device retains 95% of its initial PCE. In contrast, PBDT-TAZ:NOE0 device retains 85% of its initial PCE after 200 hours, and PBDT-TAZ:ITIC and PBDT-TAZ:PCBM retain less than 70% of their initial PCE after 100 hours. These results clearly demonstrate the superiority of NOE10 over other electron acceptors in device stability.

Further, the device stability of PBDT-TAZ:NOE10 was compared with two highly efficient solar cells PBDB-T:ITIC[27a] and PCE11:PCBM[27b] under continuous thermal aging. The normalized device performances of these solar cells with 65 °C thermal aging are shown in Figure 10b, and the detailed device parameters (V_{oc}, J_{sc}, and FF) are provided in Figure S14 (Supporting Information). After 300 hours continuous thermal aging at 65 °C, the PBDT-TAZ:NOE10 device retains >97% of its initial PCE without burn-in efficiency loss at all. The burn-in free feature of PBDT-TAZ:NOE10 device can be

attributed to its stable blend morphology.[26b] However, the PBDB-T:ITIC and PCE11:PCBM devices show significant burn-in efficiency losses with less than 80% of their initial PCEs being retained after 300 hours aging for PBDB-T:ITIC device and 100 hours aging for PCE11:PCBM device. Overall, the all-PSCs based on NOE10 show excellent storage lifetime and thermal stability. In particular, the PBDT-TAZ:NOE10 cell exhibits much better thermal stability than state-of-the-art fullerene- and small molecular non-fullerene-based solar cells, demonstrating a significant advantage of NOE10 as a promising electron acceptor for practical applications of polymer solar cells.

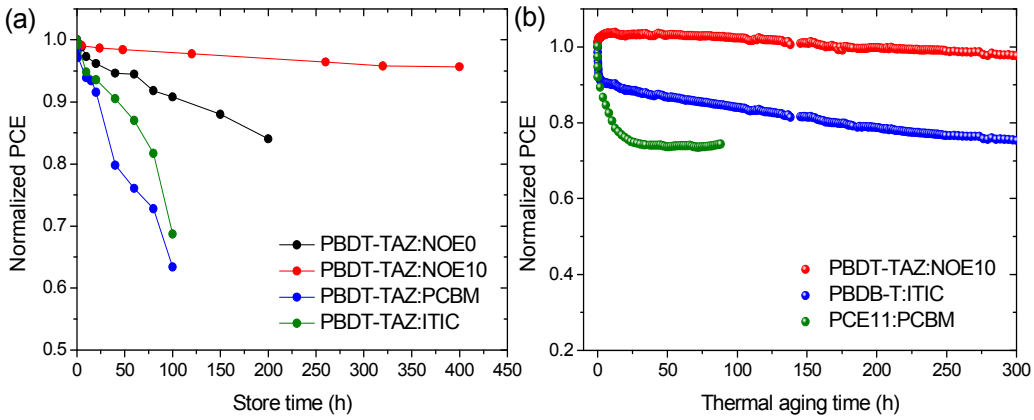

Figure 10. (a) Normalized PCE for storage lifetime of the solar cells made from the same donor polymer PBDT-TAZ but different acceptors (NOE0, NOE10, PCBM, and ITIC) in nitrogen-fill glovebox under dark; (b) normalized device performance based on PBDT-TAZ:NOE10, PBDB-T:ITIC, and PCE11:PCBM over the 65 °C thermal aging time in the dark.

■ CONCLUSION

In conclusion, we synthesized a series of NDI-based conjugated polymers (NOE*x*) modified with different contents of OE chains with the intention to fine-tune the

morphology and nanostructures of the resulting polymer:polymer BHJ blends. With 10% of OE side chains, NOE10 shows an increase of miscibility with polymer donor compared to NOE0, which renders the NOE10-based blend film with improved polymer packing, nano-phase separation, and vertical phase gradation. As a result, the best all-PSCs based on the NOE10 show a PCE of 8.1% with a J_{sc} of 12.9 mA cm^{-2} and a record high FF of 0.75. Relevant to practical applications, the all-PSCs based on NOE10 show excellent storage lifetime and thermal stability with >97% of the initial PCE after 300 hours aging at 65 °C. Indeed, NOE10 offers higher device performance than the commercial acceptor polymer N2200 when blended with different donor polymers. Our work demonstrates an effective strategy for forming optimal blend film morphology for all-PSCs, and also shows the excellent potential of NOE10 as an alternative to commercial acceptor polymer for future technological applications.

■ ASSOCIATED CONTENT

Supporting Information

Experimental details, synthetic route, GPC plots, absorption spectra, CV curves, views of surface contact measurements, PL spectra, GIWAXS patterns, RSoXS curves, FT-IR spectra, and additional tables. These materials are available free of charge via the Internet at http://pubs.acs.org.

■ AUTHOR INFORMATION

Corresponding Author

C. D. (duanchunhui@scut.edu.cn)

F. L. (fengliu82@sjtu.edu.cn)

F. H. (msfhuang@scut.edu.cn)

Notes

The authors declare non competing financial interests.

■ ACKNOWLEDGMENTS

The research was financially supported by the Recruitment Program of Global Youth Experts of China. This work was also supported by the Ministry of Science and Technology (Nos. 2017YFA0206600, 2014CB643501), and the Natural Science Foundation of China (No. 21634004, Nos. 21520102006 and 91633301). N.L. gratefully acknowledges the financial support from the DFG research grant: BR 4031/13-1, and the Bavarian Ministry of Economic Affairs and Media, Energy and Technology by funding the HI-ERN (IEK11) of FZ Jülich. C.J.B. gratefully acknowledges the financial support through the "Aufbruch Bayern" initiative of the state of Bavaria (EnCN and "Solar Factory of the Future"), the Bavarian Initiative "Solar Technologies go Hybrid" (SolTech) and the SFB 953 (DFG). C.Z. would like to acknowledge the financial support from the China Scholarship Council (CSC) and the Bavarian Initiative "Solar Technologies go Hybrid" (SolTech). M.L. acknowledges the funding from the European Union's Horizon 2020 research and innovation programme under the Marie Skłodowska-Curie grant agreement No. 747422. R.A.J.J. acknowledges funding from the European Research Council under the European Union's Seventh Framework Programme

(FP/2007-2013)/ERC Grant Agreement No. 339031. X.L. thanks the China Scholarship Council (CSC) for financial support.

■ REFERENCES

(1) Facchetti, A. *Mater. Today* **2013**, *16*, 123.
(2) Kang, H.; Lee, W.; Oh, J.; Kim, T.; Lee, C.; Kim, B. J. *Acc. Chem. Res.* **2016**, *49*, 2424.
(3) Root, S. E.; Savagatrup, S.; Printz, A. D.; Rodriquez, D.; Lipomi, D. J. *Chem. Rev.* **2017**, *117*, 6467.
(4) (a) Benten, H.; Mori, D.; Ohkita, H.; Ito, S. *J. Mater. Chem. A* **2016**, *4*, 5340. (b) Zhang, X. *Acta Polym. Sin.* **2018**, *2*, 129. (c) Song, C.-P.; Qu, Y.; Liu, J.-G.; Han, Y.-C. *Acta Polym. Sin.* **2018**, *2*, 145.
(5) (a) Gao, L.; Zhang, Z.-G.; Xue, L.; Min, J.; Zhang, J.; Wei, Z.; Li, Y. *Adv. Mater.* **2016**, *28*, 1884. (b) Guo, Y.; Li, Y.; Awartani, O.; Han, H.; Zhao, J.; Ade, H.; Yan, H.; Zhao, D. *Adv. Mater.* **2017**, *29*, 1700309. (c) Zhang, Z.-G.; Yang, Y.; Yao, J.; Xue, L.; Chen, S.; Li, X.; Morrison, W.; Yang, C.; Li, Y. *Angew. Chem. Int. Ed.* **2017**, *56*, 13503. (d) Fan, B.; Ying, L.; Wang, Z.; He, B.; Jiang, X.; Huang, F.; Cao, Y. *Energy Environ. Sci.* **2017**, *10*, 1243. (e) Li, Z.; Xu, X.; Zhang, W.; Meng, X.; Genene, Z.; Ma, W.; Mammo, W.; Yartsev, A.; Andersson, M. R.; Janssen, R. A. J.; Wang, E. *Energy Environ. Sci.* **2017**, *10*, 2212. (f) Fan, B.; Ying, L.; Zhu, P.; Pan, F.; Liu, F.; Chen, J.; Huang, F.; Cao, Y. *Adv. Mater.* **2017**, 1703906. (g) Chen, D.; Yao, J.; Chen, L.; Yin, J.; Lv, R.; Huang, B.; Liu, S.; Zhang, Z.-G.; Yang, C.; Chen, Y.; Li, Y. *Angew. Chem. Int. Ed.* **2018**, *57*, 4580. (h) Li, Z.; Fan, B.; He, B.; Ying, L.; Zhong, W.; Liu, F.; Huang, F.; Cao, Y. *Sci. China Chem.* **2018**, *61*, 427. (i) Fan, B.; Zhu, P.; Xin, J.; Li, N.; Ying, L.; Zhong, W.; Li, Z.; Ma, W.; Huang, F.; Cao, Y. *Adv. Energy Mater.* **2018**, 1703085.
(6) (a) Zhao, W.; Li, S.; Yao, H.; Zhang, S.; Zhang, Y.; Yang, B.; Hou, J. *J. Am. Chem. Soc.* **2017**, *139*, 7148. (b) Zhang, S.; Qin, Y.; Zhu, J.; Hou, J. *Adv. Mater.* **2018**, 1800868.
(7) Li, Z.; Xu, X.; Zhang, W.; Meng, X.; Ma, W.; Yartsev, A.; Inganäs, O.; Andersson, M. R.; Janssen, R. A. J.; Wang, E. *J. Am. Chem. Soc.* **2016**, *138*, 10935.
(8) (a) Kang, H.; Uddin, M. A.; Lee, C.; Kim, K.-H.; Nguyen, T. L.; Lee, W.; Li, Y.; Wang, C.; Woo, H. Y.; Kim, B. J. *J. Am. Chem. Soc.* **2015**, *137*, 2359. (b)Li, Z.; Zhang, W.; Xu, X.; Genene, Z.; Rasi, D. D. C.; Mammo, W.; Yartsev, A.; Andersson, M. R.; Janssen, R. A. J.; Wang, E. *Adv. Energy Mater*. **2017**, *7*, 1602722.
(9) (a) Jung, J. W.; Jo, J. W.; Chueh, C.-C.; Liu, F.; Jo, W. H.; Russell, T. P.; Jen, A. K.-Y. *Adv. Mater.* **2015**, *27*, 3310. (b) Hwang, Y.-J.; Courtright, B. A. E.; Ferreira, A. S.; Tolbert, S. H.; Jenekhe, S. A. *Adv. Mater.* **2015**, *27*, 4578. (c) Oh, J.; Kranthiraja, K.; Lee, C.; Gunasekar, K.; Kim, S.; Ma, B.; Kim, B. J.; Jin, S.-H. *Adv. Mater.* **2016**, *28*, 10016. (d) Kim, T.; Kim, J.-H.; Kang, T. E.; Lee, C.; Kang, H.; Shin, M.; Wang, C.; Ma, B.; Jeong, U.; Kim,

T.-S.; Kim, B. J.; *Nat. Commun.* **2015**, *6*, 8547. (e) Shi, S.; Yuan, J.; Ding, G.; Ford, M.; Lu, K.; Shi, G.; Sun, J.; Ling, X.; Li, Y.; Ma, W. *Adv. Funct. Mater.* **2016**, *26*, 5669. (f) Li, K.; Xie, R.; Zhong, W.; Lin, K.; Ying, L.; Huang, F.; Cao, Y. *Sci. China Chem.* **2018**, *61*, 576.
(10) (a) Zhan, X.; Tan, Z.; Domercq, B.; An, Z.; Zhang, X.; Barlow, S.; Li, Y.; Zhu, D.; Kippelen, B.; Marder, S. R. *J. Am. Chem. Soc.* **2007**, *129*, 7246. (b) Guo, Y.; Li, Y.; Awartani, O.; Zhao, J.; Han, H.; Ade, H.; Zhao, D.; Yan, H. *Adv. Mater.* **2016**, *28*, 8483. (c) Li, S.; Zhang, H.; Zhao, W.; Ye, L.; Yao, H.; Yang, B.; Zhang, S.; Hou, J. *Adv. Energy Mater*. **2016**, *6*, 1501991. (d) Xiong, W.-T.; Guo, Y.-K.; Zhao, D.-H.; Sun, Y.-M. *Acta Polym. Sin.* **2018**, *2*, 315.(11) Wang, Y.; Yan, Z.; Guo, H.; Uddin, M. A.; Ling, S.; Zhou, X.; Su, H.; Dai, J.; Woo, H. Y.; Guo, X. *Angew. Chem. Int. Ed.* **2017**, *56*, 15304.
(12) Long, X.; Ding, Z.; Dou, C.; Zhang, J.; Liu, J.; Wang, L. *Adv. Mater.* **2016**, *28*, 6504.
(13) Liu, S.; Firdaus, Y.; Thomas, S.; Kan, Z.; Cruciani, F.; Lopatin, S.; Bredas, J.-L.; Beaujuge, P. M. *Angew. Chem. Int. Ed.* **2018**, *57*, 531.
(14) Yan, H.; Chen, Z.; Zheng, Y.; Newman, C.; Quinn, J. R.; Dötz, F.; Kastler, M.; Facchetti, A. *Nature* **2009**, *457*, 679.
(15) (a) Chang, W.-H.; Gao, J.; Dou, L.; Chen, C.-C.; Liu, Y.; Yang, Y. *Adv. Energy Mater*. **2014**, *4*, 1300864. (b) Meng, B.; Song, H.; Chen, X.; Xie, Z.; Liu, J.; Wang, L. *Macromolecules* **2015**, *48*, 4357. (c) Chen, X.; Zhang, Z.; Ding, Z.; Liu, J.; Wang, L. *Angew. Chem. Int. Ed.* **2016**, *55*, 10376. (d) Liu, X.; Xie, B.; Duan, C.; Wang, Z.; Fan, B.; Zhang, K.; Lin, B.; Colberts, F. J. M.; Ma, W.; Janssen, R. A. J.; Huang, F.; Cao, Y. *J. Mater. Chem. A* **2018**, *6*, 395.
(16) The synthesis of this polymer will be published elsewhere.
(17) (a) Bartesaghi, D.; Pérez, I. d. C.; Kniepert, J.; Roland, S.; Turbiez, M.; Neher, D.; Koster, L. J. A. *Nat. Commun.* **2015**, *6*, 7083. (b) Gasparini, N.; Jiao, X.; Heumueller, T.; Baran, D.; Matt, G. J.; Fladischer, S.; Spiecker, E.; Ade, H.; Brabec, C. J.; Ameri, T. *Nat. Energy* **2016**, *1*, 16118.
(18) Scharber, M. C.; Mühlbacher, D.; Koppe, M.; Denk, P.; Waldauf, C.; Heeger, A. J.; Brabec, C. J. *Adv. Mater.* **2006**, *18*, 789.
(19) Zhang, C.; Mumyatov, A.; Langner, S.; Perea, J. D.; Kassar, T.; Min, J.; Ke, L.; Chen, H.; Gerasimov, K. L.; Anokhin, D. V.; Ivanov, D. A.; Ameri, T.; Osvet, A.; Susarova, D. K.; Unruh, T.; Li, N.; Troshin, P.; Brabec, C. J. *Adv. Energy Mater.* **2017**, *7*, 1601204.
(20) Owens, D. K.; Nemours E. I.; Film, S. *J. Appl. Polym. Sci.* **1969**, *13*, 1741.
(21) (a) Grulke, E. A. in *Polymer Handbook (4th Edition)*, (Eds: Brandrup, J.; Immergut, E. H.; Grulke, E. A.), Wiley, New York, USA **1999**, p. 675. (b) Kouijzer, S.; Michels, J. J.; Berg, M. v. d.; Gevaerts, V. S.; Turbiez, M.; Wienk, M. M.; Janssen, R. A. J. *J. Am. Chem. Soc.* **2013**, *135*, 12057. (c) Franeker, J. J. v.; Hermida-Merino, D.; Gommes, C.; Arapov, K.; Michels, J. J.; Janssen, R. A. J.; Portale, G. *Adv. Funct. Mater.* **2017**, *27*, 1702516. (d) Nilsson, S.; Bernasik, A.; Budkowski, A.; Moons, E. *Macromolecules* **2007**, *40*, 8291.
(22) Koster, L. J. A.; Smits, E. C. P.; Mihailetchi, V. D.; Blom, P. W. M. *Phys. Rev. B* **2005**,

72, 085205.
(23) Cowan, S. R.; Roy, A.; Heeger, A. J. *Phys. Rev. B* **2010**, *82*, 245207.
(24) Rajapaksa, I.; Uenal, K.; Wickramasinghe, H. K. *Appl. Phys. Lett.* **2010**, *97*, 073121.
(25) (a) Jahng, J.; Fishman, D. A.; Park, S.; Nowak, D. B.; Morrison, W. A.; Wickramasinghe, H. K.; Potma, E. O. *Acc. Chem. Res.* **2015**, *48*, 2671. (b) Qiu, B.; Xue, L.; Yang, Y.; Bin, H.; Zhang, Y.; Zhang, C.; Xiao, M.; Park, K.; Morrison, W.; Zhang, Z.-G. Li, Y. *Chem. Mater.* **2017**, *29*, 7543. (c) Gu, K. L.; Zhou, Y.; Morrison, W. A.; Park, K.; Park, S.; Bao, Z. *ACS Nano* **2018**, *12*, 1473.
(26) (a) Zhang, C.; Mumyatov, A.; Langner, S.; Perea, J. D.; Kassar, T.; Min, J.; Ke, L.; Chen, H.; Gerasimov, K. L.; Anokhin, D. V.; Ivanov, D. A.; Ameri, T.; Osvet, A.; Susarova, D. K.; Unruh, T.; Li, N.; Troshin, P.; Brabec, C. J. *Adv. Energy Mater.* **2017**, *7*, 1601204. (b) Li, N.; Perea, J. D.; Kassar, T.; Richter, M.; Heumueller, T.; Matt, G. J.; Hou, Y.; Güldal, N. S.; Chen, H.; Chen, S.; Langner, S.; Berlinghof, M.; Unruh, T.; Brabec, C. J. *Nat. Commun.* **2017**, *8*, 14541.
(27) (a) Zhao, W.; Qian, D.; Zhang, S.; Li, S.; Inganäs, O.; Gao, F.; Hou, J. *Adv. Mater.* **2016**, *28*, 4734. (b) Liu, Y. H.; Zhao, J. B.; Li, Z. K.; Mu, C.; Ma, W.; Hu, H. W.; Jiang, K.; Lin, H. R.; Ade, H.; Yan, H. *Nat. Commun.* **2014**, *5*, 5293.

TOC

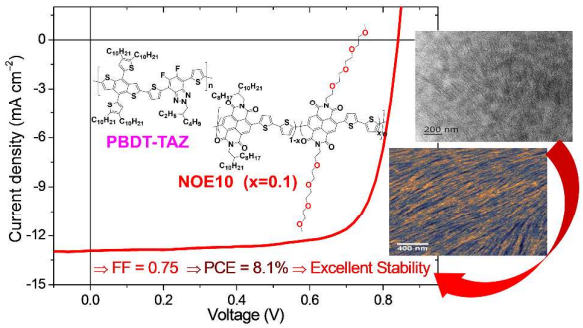
Current density (mA cm^{-2})
0
-3
-6
-9
-12
-15
0.0
0.2
0.4
0.6
0.8
Voltage (V)
PBDT-TAZ
NOE10 (x=0.1)
200 nm
400 nm
⇒ FF = 0.75 ⇒ PCE = 8.1% ⇒ Excellent Stability